Dynamic screening of fast ions moving in solids

J. D. Fuhr and V. H. Ponce
Centro Atómico Bariloche and Instituto Balseiro, Comisión Nacional de Energía Atómica and Universidad Nacional de Cuyo, 8400 Bariloche, Argentina

F. J. García de Abajo
Departamento de Ciencias de la Computación e Inteligencia Artificial, Facultad de Informática, UPV/EHU, Apartado 649, 20080 San Sebastián, Spain

P. M. Echenique
Departamento de Física de Materiales, Facultad de Química, UPV/EHU, Apartado 1072, 20080 San Sebastián, Spain
(Received 3 April 1997; revised manuscript received 26 June 1997)

The electron charge polarization induced by a fast ion moving on a solid medium is considered in a linear response model. An inhomogeneous electron gas model is introduced to describe the contribution to this dynamic screening by the bound target electrons. The action of the bound electrons is to increase the effective number of electrons of the uniform electron gas that reproduces features of the induced potential. We find that the value of the induced potential at the ion position is equivalent to that produced by a jellium of a given density, smaller than that required for the jellium to reproduce the value of the induced electric field at the ion. For the case of fast bare charges we find the precise value of jellium densities required to describe the experimental values of the stopping power in several solid targets. For the case of hydrogenic Kr projectiles in a Cu target, the mixing of its $n=3$ states by the induced potential is just that required to explain recent measurements of radiative decay. [S0163-1829(98)05212-6]

I. INTRODUCTION

A fast heavy ion moving in a solid target produces a charge polarization in the medium that acts back on the ion as an induced potential.[1] This, also called wake potential, gives the reaction of the medium to the motion of the ion, and through its gradient at the ion position defines the electric field that produces the slowing down of the projectile. The bound electron states on the ion are also mixed by the wake potential, producing a shift and splitting of the energy of the levels.

The linear response approximation (LRA) considers the action of the effective potential produced by the external charge Z to first order of perturbation;[2,3] this approximation is justified for high projectile velocities v, such that $Z/v<1$. The slowing down of the projectile is just a local effect of the wake potential. When the electrons of the solid that give rise to the wake potential can be assumed to be a uniform gas of free particles, the retarding force given by the electric field acting on Z approaches the value, in the limit $Z\omega_p/v\ll 1$:

$$Z\cdot\mathbf{E}_0\equiv Z\cdot\mathbf{E}(\mathbf{R}=\mathbf{v}t)\simeq-\hat{v}\cdot Z^2\omega_p^2\,\ln(2v^2/\omega_p)/v^2 \quad (1)$$

for $Z\omega_p/v\ll 1$, where it is assumed that the ion follows a classical trajectory and ω_p is the plasma frequency of the electrons. The assumption of free active electrons is additional to the LRA.

The characteristic length of variation of the wake potential is given by $\lambda=2\pi v/\omega_p$, so for hydrogenic projectile bound states such that the orbital radius is $n^2/Z\ll v/\omega_p$, the energy levels shift in the constant amount given by the local value of the potential at Z that for $Z\omega_p/v\ll 1$ goes to

$$-\Phi_{\mathrm{ind},0}\equiv-\Phi_{\mathrm{ind}}(\mathbf{R}=\mathbf{v}t)\simeq Z\pi\omega_p/(2v). \quad (2)$$

The mixing of hydrogenic orbitals $\phi_{nj\ell m}$ can also be described by the values of successive derivatives of the wake potential at the ion position. The Stark coupling for $\Delta\ell=1$ is produced in the approximation of localized orbitals by the electric field $\mathbf{E}_0$; quadrupolar couplings $\Delta\ell=2$ are given by $\nabla_r^2\Phi_{\mathrm{ind}}(\mathbf{r}=\mathbf{v}t)$, and so on. For states with large n the Taylor expansion of Φ_{ind} implicit in results 1,2 is no longer valid, so the detailed form of the wake potential is required to get the dynamic mixing of states:

$$\begin{aligned}\langle\phi_{nj\ell m}|-\Phi_{\mathrm{ind}}(\mathbf{r})|\phi_{n'j'\ell'm'}\rangle&\\ \approx-\langle\phi_{nj\ell m}|\Phi_{\mathrm{ind},0}+\mathbf{E}_0\cdot\mathbf{r}+\tfrac{1}{2}\nabla_r^2\Phi_{\mathrm{ind},0}\cdot r_i r_j&\\ +\cdots|\phi_{n'j'\ell'm'}\rangle.&\end{aligned} \quad (3)$$

Müller and Burgdörfer[4] have studied the energy shift of hydrogenic levels beyond the assumption of localized orbitals, by numerically solving the Schrödinger equation for the eigenstates in the combined Coulomb plus wake potentials. The upward shift of the binding energies and the level splitting of l states within a given n manifold are followed as the strength of the wake potential is increased (the collision velocity decreased), until each bound state merges into the continuum. In the present work we will consider fast and heavy projectiles, so the wake potential is a weak perturbation and the bound projectile states remain well localized in a wide range of quantum numbers $n<\sqrt{Zv/\omega_p}$.

Due to the connection just sketched of ion stopping and spectroscopy of bound levels with the induced potential

$\Phi_{\rm ind}(\mathbf{r})$, a fast heavy charge moving in solid matter is an excellent probe to check current models of the dynamic response of the electrons of the solid. There are a great number of measurements of the stopping of fast ions in solids, which provide information on the induced electric field at the ion. In recent years experiments have been performed that test the action of the wake potential on bound states of the projectile.[5–7] These measurements require projectiles with high charges and velocities and thin solid targets, in order to have long-lived bound hydrogenic states. They provide more stringent tests on the wake potential, since the state mixing with shift and splitting of levels depends, in principle, on the detailed form of $\Phi_{\rm ind}(\mathbf{r})$.

The wake potential describes the linear response of quasifree electrons of the solid to the external particle. The contribution of bound target electrons depends on the type of external perturbation. To excite or even polarize these orbitals, it is necessary to have an external probe capable of transferring the amounts required of both energy and momentum. Therefore, due to the small value of momentum carried by photons, the response to them as external excitations will come almost exclusively from the valence (quasifree) electrons of the solid. The effective number of electrons responding to charged particles will be greater than that for photons: using as projectiles with a given velocity v particles such as electrons, protons, and heavy nuclei, the maximum momentum transfer is of the order of $2v$. Therefore, bound target electrons with orbital velocities $Z_T/n<v$ can be excited, and the effective number of active electrons per target atom will be greater than the valence, quasifree electrons that give rise to the collective volume plasmon excitation of frequency ω_P. While the number of active target electrons varies with the projectile velocity, in the linear response approximation, the dependence on the charge Z of the projectile appears only as a factor Z^2 in the energy-loss cross section and stopping of the projectile.

The calculation of the response of the whole electronic system of the solid is a very difficult many-body problem. The usual approximation, of assuming that inner bound states are frozen and only valence electrons react to the external excitation, is not well justified for fast heavy projectiles.

The interaction of a fast ion with an atomic target can be described by the impulse approximation,[8] valid when the time of effective projectile-target electron interaction is small compared with the response time of the electron to the target binding force. In this context, the process is a binary collision of the charge Z and a free electron with a momentum distribution given by the initial bound orbital. The local plasma approximation (LPA) (Refs. 9 and 10) assumes that the bound electrons react as free particles to the external perturbation, and that they may be described at each point of space as a gas of free electrons with the density given by the initial target state to which they belonged. The LPA is then the impulse approximation with the additional assumption of replacing the momentum distribution of the target electrons by that of a free-electron gas with the local density of the target state.

Within the validity of the linear response model, applications of LPA to the case of photoabsorption processes produce results in excellent accord with experimental values; here it replaces the calculation of the oscillator strengths of the target, but there is no clear way to justify this approximation, even in this case where the linear response is strictly valid.[10] There are many applications of LPA to the energy loss of fast charges in solids, started by the original proposal of the model by Lindhard and co-workers.[9,11] Applications to projectiles other than ions are presented by Tung *et al.*,[12] in the calculation of electron mean free paths and energy losses in various solids. Other applications have gone beyond the assumptions of validity for the linear response description, such as estimations of contributions of order Z_P^3 to stopping.[13] More recently, the LPA has been applied to calculate the contribution to the stopping by deep bound electrons (with velocities $v_b \gg v$) (Ref. 14), which produces the results obtained in close accord with measurements. The LPA has also been applied for the definition of the valence states in radiative electron capture by channeled ions; here the very complicated electron states of the crystal are replaced by either plane or Coulomb waves with a local density, and the capture process is assumed to proceed from the plasma of free electrons found at each point of its trajectory by the channeled ion.[15]

II. APPLICATIONS

A. Fast bare projectile charges

We will study the passage of a fast heavy charge through a solid with a velocity that is higher than the characteristic speed of the deepest bound electrons of the medium. We assume that the charge Z_P moves along a classical straight line trajectory, traversing successive Wigner-Seitz cells of the solid with a uniform distribution of impact parameters, since it moves along a random crystalline direction.

Some targets of special experimental interest are those of C, Al, Cu, Ag, and Au. For the case of Cu the electron density provided by one valence electron for each atom in the solid corresponds to $r_s=2.67$ a.u., and gives a plasmon frequency $\omega_p=0.397$ a.u. (10.8 eV). If the eleven $3d$ and $4s$ electrons of the valence band are included in the density of the free electron modeling the band, we get $\omega_p=1.31$ a.u. (35.7 eV), and $r_s=1.20$ a.u. The measured plasma frequency corresponds to 3.15 active electrons per target atom,[16] pointing to a partial contribution of the $3d$ electrons to the collective response.

To incorporate the contribution of bound localized electrons to the target dynamic response we will employ the local plasma approximation. At each point $\mathbf{R}$ the charge experiences, according to LPA, a response by the target electrons described by that of a free-electron gas of local density $n(\mathbf{R})$. Replacing the Wigner-Seitz cell by a sphere, the density $n(R)$ will depend only on the radial distance R. The average induced potential is given by

$$\overline{\Phi}_{\rm ind}(\mathbf{r})=\frac{3}{R_{\rm WS}^3}\int_0^{R_{\rm WS}} dR\cdot R^2\Phi_{\rm ind}(\mathbf{r},n(R)), \tag{4}$$

where $\mathbf{r}$ is the field coordinate relative to the ion and $R_{\rm WS}$ the Wigner-Seitz sphere radius; $n(R)$ is the self-consistent electronic density of each solid target considered.[17] The free-electron gas response is given by[2]

TABLE I. Comparison of the effective number of electrons per target atom $N_{\rm eff}^{\rm LPA}(\Phi)$, $N_{\rm eff}^{\rm LPA}(\mathbf{E})$ (and corresponding effective plasma frequency $\omega_{P,\rm eff}^{\rm LPA}$, in eV) obtained in the LPA, with the number of active electrons required by measurements of stopping (Ref. 21). The plasma frequency ω_P of each material is also presented.

Target	Be	C	Al	Si	Ti	Ni	Cu	Ag
Z_T	4	6	13	14	22	28	29	47
ω_P	19.9	25.0	15.3	17.0	17.6	19.5	19.1	25.0
$\omega_{P,\rm eff}^{\rm LPA}(\Phi)$	21.76	22.47	21.36	23.76	27.22	36.22	33.72	31.23
$\omega_{P,\rm eff}^{\rm LPA}(\mathbf{E})$	24.97	29.05	29.95	27.85	36.45	52.22	50.86	52.50
$N_{\rm eff}^{\rm LPA}(\Phi)$	2.70	3.24	5.39	8.22	8.61	9.92	9.45	12.40
$N_{\rm eff}^{\rm LPA}(\mathbf{E})$	3.67	5.44	10.82	11.29	17.08	21.73	22.26	34.20
$N_{\rm eff}^{\rm Exp}(\mathbf{E})$	3.68	5.48	10.41	11.74	16.90	21.31	21.65	32.68

$$\Phi_{\rm ind}(\mathbf{r})=Z_P\int\frac{d\mathbf{q}}{(2\pi)^3}\int\frac{d\omega}{2\pi}\frac{8\pi^2}{q^2}\delta(\omega-\mathbf{q}\cdot\mathbf{v})\times\left\{\frac{1}{\varepsilon(q,\omega)}-1\right\}\exp(i\mathbf{q}\cdot\mathbf{r}-i\omega t). \tag{5}$$

The closed form random-phase approximation (RPA) $\varepsilon(q,\omega)$ for the dielectric function of an electron gas of density n will be used.[18,19]

Equations (4) and (5) determine the induced potential in the approximations of local response (LRA) and local plasma (LPA), strictly valid when $v\gg Z_P$ (LRA), and $v\gg Z_T$ (LPA). Before carrying out a numerical calculation of these expressions, it is instructive to obtain simple estimations of the induced potential and electric field at the ion position; Eqs. (1) and (2) show that the dominant dependences on the density n are

$$\Phi_{\rm ind}(0)\simeq Z_P\pi\omega_P/(2v)\simeq Z_P\pi^{3/2}n^{1/2}/v$$

and

$$\nabla_r\Phi_{\rm ind}(0)\simeq\hat{v}Z_P\omega_P^2\,\ln(2v^2/\omega_P)/v^2=\hat{v}4\pi Z_P n\,\ln(v^2/\sqrt{\pi}n)/v^2,$$

so in the LPA these are the estimations with n replaced by the effective densities:

$$\overline{n^{1/2}}=\frac{3}{R_{\rm WS}^3}\int_0^{R_{\rm WS}}dRR^2n(R)^{1/2} \tag{6}$$

to get

$$\overline{\Phi}_{\rm ind}(0)\simeq Z_P\pi^{3/2}\overline{n^{1/2}}/v \tag{7}$$

and

$$\overline{n}=\frac{3}{R_{\rm WS}^3}\int_0^{R_{\rm WS}}dRR^2n(R) \tag{8}$$

for

$$\overline{\mathbf{E}}_{\rm ind}(0)\simeq-\hat{v}4\pi Z_P\overline{n}\,\ln(v^2/\sqrt{\pi\overline{n}})/v^2. \tag{9}$$

Since $\overline{n}>(\overline{n^{1/2}})^2$, the density that determines the electric field is larger than the one corresponding to the induced potential. This indicates that *the effective number of target electrons varies with the effect observed: it is larger (inner shell target electrons more active) for the induced electric field than for the induced potential at the projectile.*

The scale factor $\sqrt{n}$ incorporated to the density dependence each time a derivation is performed on $\Phi_{\rm ind}$ just reflects the n dependence of the characteristic wavelength of the induced potential in the LRA: $\lambda\simeq 2\pi v/\omega_p=\sqrt{\pi/n}v$. This $\sqrt{n}$ factor added on successive terms of the multipole expansion of $\Phi_{\rm ind}$ produces a systematic enhancement of the weight of high-electron-density regions as we consider higher multipole terms.

Physically, this means that projectile trajectories that penetrate deep into the inner shells of the target produce a larger relative contribution to define the mean electric field than to define the induced potential. Therefore, the density of the uniform electron gas the dynamic response of which reproduces the induced electric field acting on the ion is larger than the density required to reproduce the induced potential.

We will apply in the first place the LPA to calculate the effective induced potential and electric field acting on a fast bare charge moving in a solid medium, such that $Z_T, Z_P\leqslant v$. This approach has been used in the past to obtain the stopping power of solids.[9,20] We present in Table I the LPA effective number of electrons $N_{\rm eff}^{\rm LPA}(\Phi)$, $N_{\rm eff}^{\rm LPA}(\mathbf{E})$ contributed by each target atom in order to build up the potential $\Phi_{\rm ind}(0)$ and electric field $\mathbf{E}_{\rm ind}(0)$ at the ion, respectively. We compare our results with the value $N_{\rm eff}^{\rm Exp}(\mathbf{E})$ obtained from Eq. (4) for $\overline{\mathbf{E}}_{\rm ind}(0)=-\nabla_r\overline{\Phi}_{ind}(0)$, and required to reproduce the measurements of stopping of Gauvin *et al.* for O ions with $v\simeq 33$ a.u. in several solid targets;[21] at this velocity the projectile equilibrium charge state is that of the bare nucleus.

As we see, the induced potential and electric field produced by a fast projectile correspond to higher jellium density and plasma frequency than those of the jellium that gives the plasmon excitation for each material, this last obtained through the characteristic energy loss of electrons in transmission experiments or deduced from optical data. This indicates that inner electrons do in effect play a relevant role in the stopping of a fast charge. The agreement with the number of active electrons per atom extracted from experimental results is extremely good; it starts to degrade for targets with $Z_T\geqslant v$, and this can be attributed to the failure of approximating inner shell electrons by an inhomogeneous gas of free electrons when their orbital speed is not small compared with the ion velocity. The absence of a threshold energy for in-

elastic transitions in the case of free electrons makes them easier to excite than those in tightly bound orbitals, which explains the tendency of $N_{\mathrm{eff}}^{\mathrm{LPA}}(\mathbf{E})$ to be larger than $N_{\mathrm{eff}}^{\mathrm{Exp}}(\mathbf{E})$ for heavy targets.

B. Dynamic screening on projectile bound states

We now consider the effects of the dynamical response of the target electrons on the bound electron states of a composite projectile; due to its simplicity, and to the existence of measurements, we analyze the case of hydrogenic ions. We will study a heavy ion moving along a random crystalline direction with velocity higher than the characteristic speed of the deepest bound electrons of the medium, and compare our results with experiments performed with hydrogenic Kr moving with $v=36$ a.u. in C, Al, and Cu targets.[6,7] We consider the mixing of the projectile bound orbitals due to the action of the induced potential generated by the projectile nucleus Z_P; since $Z_P \gg 1$ we will neglect the induced potential coming from the bound electron. Accounting for spin-orbit coupling, the degeneracy of each hydrogenic level for a given principal quantum number n and total angular momentum j is reduced to the allowed sets of orbital ℓ and total angular momentum projection m_j. The shift and splitting of the levels is obtained through the diagonalization of the coupling matrix $\langle \phi_{[i]}|\overline{\Phi}_{\mathrm{ind}}|\phi_{[j]}\rangle$, where $[i]=n_i j_i \ell_i m_i$.

The states mixed by the induced potential are those the energy splitting of which is smaller than or of the order of the coupling $\langle \phi_{[i]}|\overline{\Phi}_{\mathrm{ind}}|\phi_{[j]}\rangle$, and this in turn is of the order of the electric field $(Z_P\omega_P/v)^2$ for nondiagonal terms. The spin-orbit splitting is

$$\Delta E_{n,j}^{S-O}=E_{n,j}-E_{n,j-1}=-Z_P^4/[2c^2n^3(j^2-\tfrac{1}{4})]. \quad (10)$$

Therefore, for $n<(Z_P v/c\omega_P)^{2/3}$ the induced potential will only mix fine structure orbitals with the same value of total angular momentum j: $\phi_{n,j,\ell,m}$ with $\ell=j\pm\frac{1}{2}$. For the case of $v=36$ a.u. Kr projectiles this corresponds to $n<5$.

The degeneracy of the pair of $\ell=j\pm\frac{1}{2}$ states is already broken by the Lamb shift:[22]

$$\Delta E_{nj\ell}^{\mathrm{Lamb}}=E_{nj\ell}-E_{nj\ell-1}\approx\frac{1}{c}\ln\left(\frac{c}{Z_P}\right)\Delta E_{n,j}^{S-O} \quad (11)$$

so there is a range of induced potential strengths

$$\frac{1}{c}\ln\left(\frac{c}{Z_P}\right)\Delta E_{n,j}^{S-O}<(Z_P\omega_P/v)^2<\Delta E_{n,j}^{S-O}, \quad (12)$$

too weak to overcome the fine-structure splitting, but strong enough to mix states $(nj\ell=j\pm\frac{1}{2})$.

Before performing the detailed diagonalization of the coupling matrix, we will analyze the effect of the induced potential on the shift of levels (diagonal terms) and their mixing (nondiagonal terms). We said before that $2\pi v/\omega_P$ is a first estimation of its length scale of variation along the projectile trajectory,[23] but at the high velocities we are interested in the behavior of the induced potential close to the ion is markedly anysotropic. Figures 1(a) and 1(b) represent its contour lines for $v=4$ and 35 a.u.

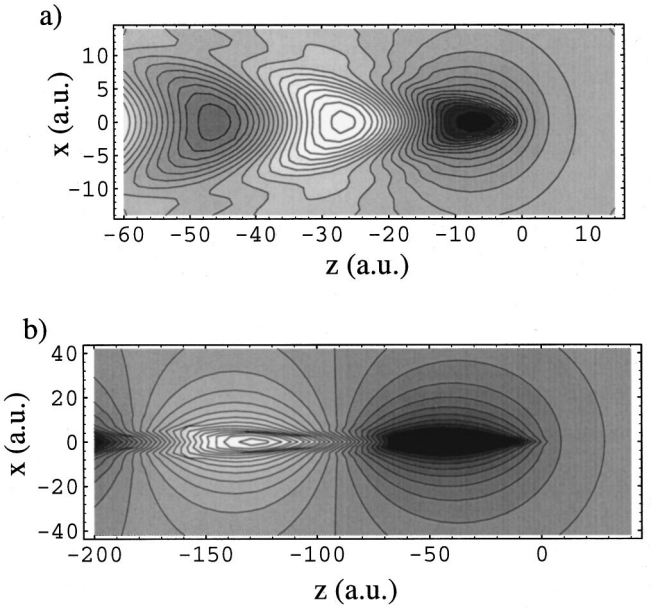

FIG. 1. Contour lines for the induced potential set up by a fast bare charge in a jellium with $r_s=1.27$ a.u., calculated for velocities (a) $v=4$ and (b) $v=36$ a.u.

Figure 1(a) shows clearly the Cerenkov-like cone region where the target electron perturbation by the passage of the ion is concentrated. This cone in Fig. 1(b) shrinks to an aperture of the order of $v_F/v\simeq 0.03$ radians for typical metals. We also see that Φ_{ind} grows linearly approaching Z_P from behind, reaching a small negative value and then remaining small while going to zero ahead of the projectile. Translating this to electric-field values, $\hat{v}\cdot\mathbf{E}_{\mathrm{ind}}(z)$ remains close to a constant behind the ion, and drops rapidly to zero ahead of it. Furthermore, the location of the bulk of target polarization in the Cerenkov cone produces a stronger drop of induced potential in the direction normal to the trajectory than along it, as already noticed before.[23,19]

Taking into account the above-mentioned considerations, we make a first estimate of the energy shift and dipole coupling between some of the bound hydrogenic states on Z_P, assuming them to be so localized that the matrix elements $\overline{M_{n\ell m}^{n\ell' m'}}=\langle \phi_{[i]}|\overline{\Phi}_{\mathrm{ind}}|\phi_{[j]}\rangle$ are described by the first nonzero contributions of the Taylor expansion (3) of $\overline{\Phi}_{\mathrm{ind}}$. Since diagonal terms become independent of the state ϕ considered, there is an upward shift of the energy levels given by

$$\Delta E_L=\overline{\Phi}_{\mathrm{ind}}(0) \quad (13)$$

while nondiagonal terms with $\Delta\ell=1$ have a linear Stark form

$$\overline{M_{n\ell m}^{n\ell' m'}}_L=\mathbf{E}_{\mathrm{ind}}(0)\cdot\langle \phi_{njlm}|\mathbf{r}|\phi_{nj\ell' m}\rangle \quad (14)$$

in the $nj\ell m$ basis.

The fine-structure states $\phi_{n,j,\ell,m}$ are a linear combination of the hydrogenic orbitals with well-defined orbital momentum ℓ: $\chi_{n\ell m_s}$ with $\ell=j\pm\frac{1}{2}$. The coupling matrix can then be presented in the $(n\ell m)$ basis: $\overline{M_{n\ell m}^{n\ell' m'}}$, the transformation to the $(nj\ell m)$ basis being straightforward.

TABLE II. Diagonal (S states) and dipole ($S \rightarrow P$) matrix elements of the induced potential for a hydrogenic Kr atom moving with $v=36$ a.u. in a jellium gas with density corresponding to $r_s=2$ a.u. The first row for each quantum number n corresponds to the full calculation, the second to the approximation of localized orbitals; notice that the diagonal matrix element of $\bar{\Phi}_{\rm ind}$ in the approximation of localized orbitals is independent of the state n.

n	$\langle n00\vert\bar{\Phi}_{\rm ind}\vert n00\rangle$	$\langle n00\vert\bar{\Phi}_{\rm ind}\vert n10\rangle$
2	0.98861	0.0060757
	0.98940	0.0076830
3	0.98709	0.013171
		0.018662
4	0.98544	0.021618
		0.034089
5	0.98341	0.030620
		0.053745
6	0.98014	0.039185
		0.078131
7	0.99121	0.042305
		0.106750

We have performed a calculation for the coupling matrix using the full form of $\bar{\Phi}_{\rm ind}(\mathbf{r})$, given by Eqs. (4) and (5). We proceed first to check the validity of the approximations, Eqs. (13) and (14), that predict a shift in the block of energy levels and dipole couplings, as those produced by an homogeneous electric field. Table II compares diagonal $\overline{M^{n00}_{n00}}$ and dipole $\overline{M^{n10}_{n00}}$ matrix elements with the predictions [Eqs. (13) and (14)] of the approximation by localized orbitals.

We see that the mean value of the induced potential is quite well reproduced by the assumption of localized orbitals. Figure 2 shows the reason for this: even though the contour lines of $\bar{\Phi}_{\rm ind}(\mathbf{r})$ show a marked anisotropy, they are

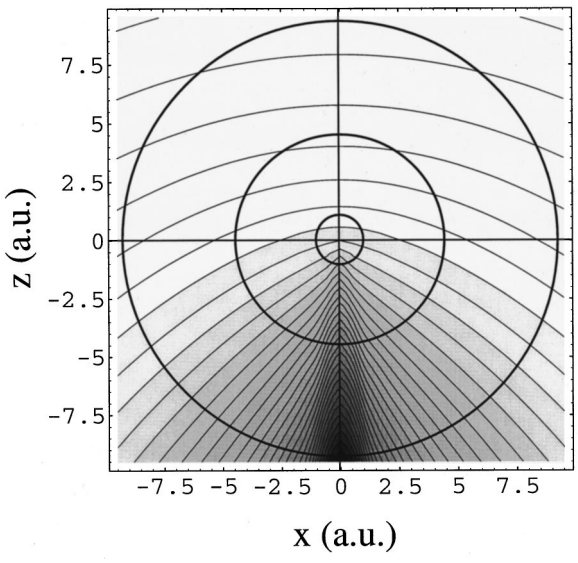

FIG. 2. Contour lines of the induced potential close to the projectile, compared with the extension of bound hydrogenic states represented by the mean orbital radius $\sqrt{\langle\phi_{n\ell m}\vert r^2\vert\phi_{n\ell m}\rangle}$. Contour lines are drawn at 0.003 intervals, and the value of that passing at the projectile is 0.054.

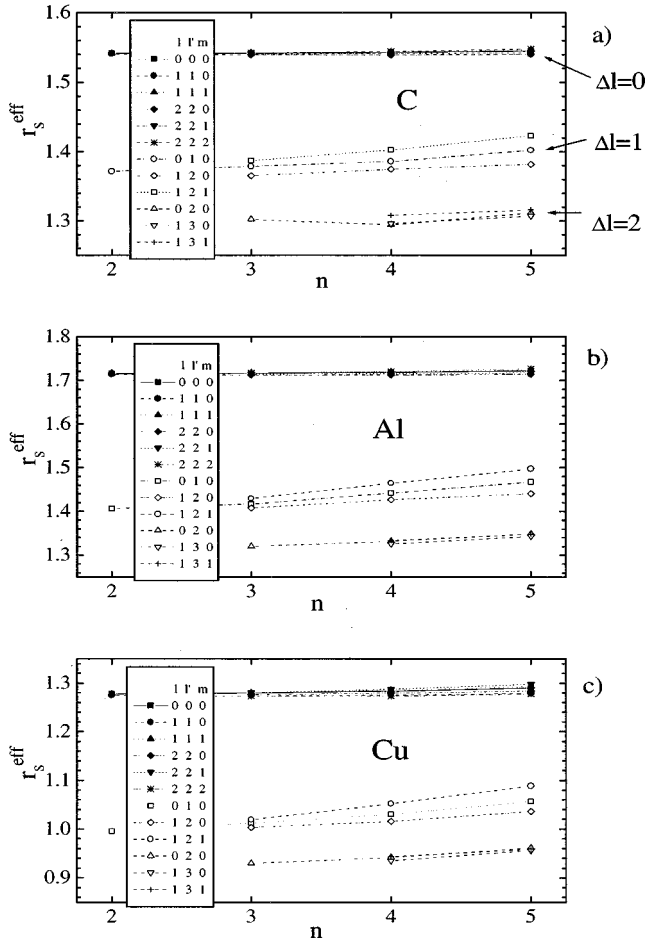

FIG. 3. Intrashell coupling elements for hydrogenic orbitals on a Kr nucleus, moving with $v=36$ a.u. in (a) carbon, (b) aluminum, and (c) copper solid targets. The coupling is expressed in terms of the density of the jellium target that would produce the same value for the matrix element. The density is expressed as both the electronic volume radius r_s and the plasma frequency ω_P of the jellium. Only orbitals with $n\leqslant 5$ and $\ell\leqslant 3$, and coupling elements with $\Delta\ell\leqslant 2$ have been considered.

mounted on a large mean value of this potential. On the other hand, for the dipole elements that depend on the gradient of the potential, the approximation of localized orbitals gives wrong values even for the $(200)\rightarrow(210)$ coupling. The anisotropy of $\bar{\Phi}_{\rm ind}(\mathbf{r})$ points to a strong spatial dependence of the induced electric field, responsible for the growing departure with n of this approximation from the correct values as seen in Table II.

We show in Figs. 3(a)–(c) the coupling produced by the induced potential for states with the same n ($1\leqslant n\leqslant 5$), and $\ell=0,1,2,3$. The targets are C, Al, and Cu.

What we get from these results is a clear confirmation, and generalization, of what we found before for bare charges about the dependence of the number of effective target electrons that participate in producing different features of the induced potential. We already noticed in Table I that $N_{\rm eff}^{\rm LPA}(\Phi)$ is smaller than $N_{\rm eff}^{\rm LPA}(\mathbf{E})$, this indicating that small impact parameter projectile-target ion collisions participate with a higher weight in determining the induced electric field than the induced potential. Now we see that the coupling between orbitals with $\Delta\ell=2$ that depends basically on the

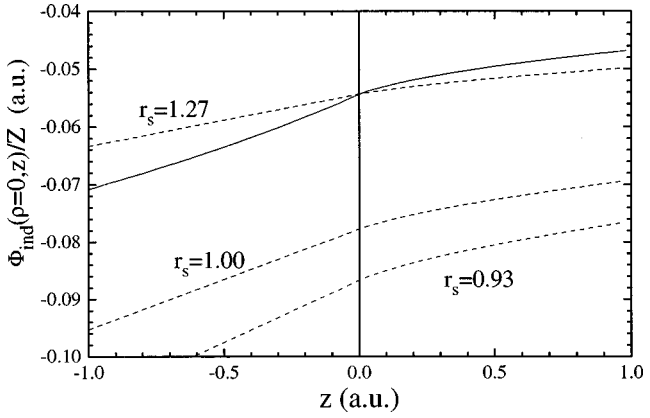

FIG. 4. Induced potential along the velocity direction per unit charge of a projectile with velocity $v=36$ a.u. in a Cu target. Full line: calculated with LPA. Dashed line: for jellium with three densities that correspond to the effective number of active electrons that give the same $\Phi_{\rm ind}$, $\mathbf{E}_{\rm ind}$, and $\partial^2\Phi_{\rm ind}/\partial z^2$ as LPA at the ion position.

second derivatives $\partial^2\Phi_{\rm ind}/\partial x_i x_j$ corresponds to a larger number of active electrons, pointing to a greater dominance of close collisions in producing these types of intrashell coupling (and transitions). The effective jellium density that describes the induced potential at the ion position has been found to be smaller than the density of the jellium that reproduces the induced electric field at the ion, and this in turn is smaller than that required to generate the quadrupole coupling $\partial^2\Phi_{\rm ind}/\partial r_i r_j$ between bound states at the ion. A picture of this varying efficiency of target electrons in setting up different features of the dynamic screening is shown in Fig. 4; it presents induced potentials along the direction of ion motion, they correspond to the LPA calculation resulting from the average of electron density along the ion trajectories [Eq. (4)], and to three jelliums with densities that reproduce each one of them either the induced potential, or its first or its second derivatives at the ion position.

As a final result of this section we have diagonalized the coupling matrix $\langle\psi_{n,j,\ell,m}|\Phi_{\rm ind}|\psi_{n,j',\ell',m'}\rangle$ in the $nj\ell m$ basis to obtain the splitting of levels produced by the dynamic screening on a Kr hydrogenic ion moving with $v=36$ a.u. in Cu. In Fig. 5 we present the first excited levels with spin-orbit and Lamb splitting, and the mixing by the induced potential.

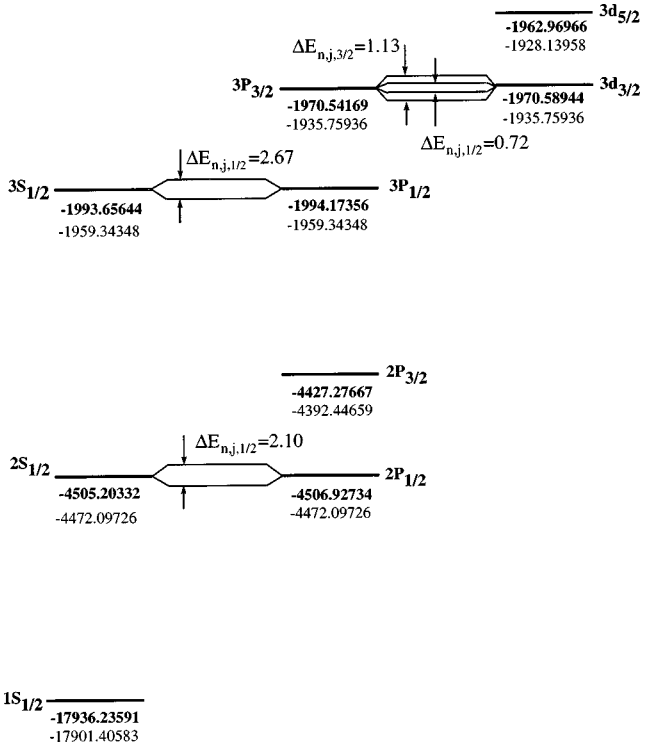

FIG. 5. Energy levels for a hydrogenic Kr ion, including fine structure and Lamb shifts, and state mixing by the induced potential set up by the ion moving with $v=36$ a.u. in a Cu target described by the LPA approximation. Bold data: isolated Kr^{35+} levels. Standard data: Shifted energy levels (energy in eV).

III. COMPARISON WITH EXPERIMENTAL RESULTS

The experiments of Rozet *et al.*,[5] Nicolai *et al.*,[6] and Despiney and co-workers[7,24] send fast bare Kr ions on thin solid foils of C, Al, and Cu. The probability of capturing an electron in some excited bound hydrogenic state is small, of the order of 0.1. The one-electron ions formed decay to the ground level emitting radiation. The intensity of the x rays indicates the population of the states participating in the cascade. Apart from the feeding of each state through the electron capture and radiative channels, there are collisional intrashell (and intershell) transitions, that play a non-negligible role in a description of the x-ray intensity. Experimental results of the relative intensity of Lyman α, β, γ, and δ rays emitted and measured as a function of the target thickness can be interpreted, for each solid target, in terms of a set of intrashell and intershell collisional mixing, and radiative deexcitation cascades. Even though intershell collisional transitions are not well known, there is a set of proposed values for these cross sections that produce a close agreement with the measured Lyman intensities.

On the other hand, for the case of Cu targets Balmer α line intensities depend on the population of $n=3$ states. A model (collisional model[25]) follows the evolution of these populations, incorporating electron capture and loss by the projectile, collisional mixing and radiative transitions, but it is not able to reproduce the experimental intensities of these x rays. As the levels $(3s_{1/2},3p_{1/2})$ and $(3p_{3/2},3d_{3/2})$ are coherently mixed by the wake potencial, their amplitudes do not evolve as those of independent states; instead a pattern of destructive and constructive interferences appears in the population of each state. This beating is observed as oscillations in the intensity of the measured x rays as a function of the target foil. The value of the coupling produced by the induced potencial [see Fig. 4(c)] is the one required to reproduce the measured target thickness dependence of the intensity and wavelength of these oscillations, once a correction is introduced to the phases of the capture amplitudes to the $n=3$ states, calculated in the continuum distorted wave approximation.

To reproduce the measurements of Despiney,[7] the coupling by the induced potential of $3s_{1/2}$ and $2p_{3/2}$ states should correspond to an electric field produced by a jellium of $r_s=0.99$ a.u. ($\omega_P=48$ eV). If we look in Fig. 3(c) at the matrix element between the hydrogenic (n,ℓ,m) orbitals

$(3,0,0)\leftrightarrow(3,1,0)$, we get a coupling of these orbitals corresponding to an effective density with $r_s=1.01$ a.u. ($\omega_P=46.4$ eV), in excellent accord with the required value. This effective electron density is close to but smaller than the one obtained by us for the local value of the electric field at the nucleus, $r_s=0.95$ a.u. ($\omega_P=50.86$ eV); the difference comes from contributions to the matrix element $\overline{M_{300}^{310}}$ of higher-order terms of the Taylor expansion of $\Phi_{\rm ind}$, Eq. (3).

By looking at the case of Al targets, Fig. 3(b), we see that there is also a contribution from inner shell Al electrons to the effective electron density producing the Stark-like coupling of projectile bound states. In the specific case of $(3,0,0)\leftrightarrow(3,1,0)$ mixing, this gives $r_s^{\rm eff}=1.42$ ($\omega_p=27.8$ eV), while the usual free-electron model for Al considers $r_s=2.07$ ($\omega_p=15.82$ eV). Therefore, the intensities of the x-ray lines originating in the $3s_{1/2}$ and $2p_{3/2}$ states of Kr projectiles in Al are also affected by the dynamic response of inner $(1s,2s,2p)$ target electrons.

In the case of C targets, as we see in Fig. 3(a) the response of inner shell electrons to the Kr projectile is less important. In fact, four electrons of C are usually incorporated into the free-electron model of the solid ($r_s=1.53$ for graphite); this leaves only two $1s$ electrons in passive frozen states. To reproduce the experimental results for the Balmer lines it is necessary to take into account, as for the Cu target, the wake mixing of $(3s_{1/2},3p_{1/2})$ and $(3p_{3/2},3d_{3/2})$ levels. The intensities of these couplings given in Fig. 4(a), are the ones that, together with the collisional model and phase correction of the CDW capture amplitudes, produce a close agreement with measurements of Despiney.[7,24]

IV. CONCLUSIONS

In summary, we have used the local plasma approximation (LPA) to describe inner and valence electrons of a solid by a jellium model with space-dependent density. We have calculated the dynamic screening of fast heavy ions by the target electrons in the linear response approximation. We find that the effective number of electrons per target atom interacting with the ion depends strongly on the effect observed: the self-energy of the ion as a fast bare charge, given by the induced potential at the ion position, corresponds to a number of active electrons that is smaller than that producing the slowing force at the ion, given by the induced electric field. In the case of a localized hydrogenic ion as projectile, the induced potential at the nucleus $\Phi(0)$ represents the energy shift of the bound state, the electric field gives the dipole transitions produced by the dynamic screening, and second derivatives of the potential cause quadrupole transitions. In this approximation we find the sequence of increasing number of active electrons: $N_{\rm eff}^{\rm LPA}(\Phi)<N_{\rm eff}^{\rm LPA}(\nabla\Phi)N_{\rm eff}^{\rm LPA}(\nabla^2\Phi)$. A full calculation of the coupling terms shows that the approximation of localized orbitals fails even for tightly bound states. Nevertheless, the multipole matrix elements again show the sequence of increasing number of active electrons: $N_{\rm eff}^{\rm LPA}(\Delta\ell=0)<N_{\rm eff}^{\rm LPA}(\Delta\ell=1)<N_{\rm eff}^{\rm LPA}(\Delta\ell=2)$, as shown in Fig. 3.

ACKNOWLEDGMENTS

The authors acknowledge help and support by the Departamento de Educación del Gobierno Vasco, Gipuzkoako Foru Aldundia, and the Spanish Comisión Asesora Científica y Técnica (CAICYT).

[1] J. Neufeld and R. H. Ritchie, Phys. Rev. **98**, 1632 (1955); **99**, 1125 (1955).
[2] P. M. Echenique, F. Flores, and R. H. Ritchie, *Solid State Physics*, edited by H. Ehrenreich and D. Turnbull (Academic, New York, 1990), Vol. 43, p. 229.
[3] P. M. Echenique, F. J. García de Abajo, V. H. Ponce, and M. E. Uranga, Nucl. Instrum. Methods Phys. Res. B **96**, 583 (1995).
[4] J. Muller and J. Burgdorfer, Phys. Rev. A **43**, 6027 (1991).
[5] J. P. Rozet, A. Chetioui, P. Bouisset, D. Vernhet, K. Wohrer, and A. Touati, Phys. Rev. Lett. **58**, 337 (1987).
[6] P. Nicolai, M. Chabot, J. P. Rozet, M. F. Politis, A. Chetioui, C. Stephan, A. Touati, D. Vernhet, and K. Wohrer, J. Phys. B **23**, 3609 (1990).
[7] I. Despiney, Ph.D. thesis, Universite Pierre et Marie Curie, Paris, 1994.
[8] M. R. C. Mc Dowell and J. P. Coleman, *Introduction to the Theory of Ion-Atom Collisions* (North-Holland, Amsterdam, 1970); see p. 294.
[9] J. Lindhard and M. Scharff, K. Dan. Vidensk. Selsk. Mat. Fys. Medd. **27**, No. 15 (1953).
[10] R. E. Johnson and M. Inokuti, Comments At. Mol. Phys. **14**, 19 (1984).
[11] E. Bonderup, K. Dan. Vidensk. Selsk. Mat. Fys. Medd. **35**, No. 17 (1967).
[12] C. J. Tung, J. C. Ashley, and R. H. Ritchie, Surf. Sci. **81**, 427 (1979).
[13] J. C. Ashley, R. H. Ritchie, and W. Brandt, Phys. Rev. B **5**, 2393 (1972).
[14] J. Calera-Rubio, A. Gras-Marti, and N. R. Arista, Nucl. Instrum. Methods Phys. Res. B **93**, 137 (1994).
[15] J. M. Pitarke, R. H. Ritchie, and P. M. Echenique, Phys. Rev. B **43**, 62 (1991).
[16] C. J. Powell, Proc. Phys. Soc. London **76**, 593 (1960).
[17] V. L. Moruzzi, J. F. Janak, and A. R. Williams, *Calculated Electron Properties of Metals* (Pergamon Press, New York, 1978).
[18] J. Lindhard, K. Dan. Vidensk. Selsk. Mat. Fys. Medd. **28**, No. 8 (1954).
[19] A. Mazarro, P. M. Echenique, and R. H. Ritchie, Phys. Rev. B **27**, 4117 (1983).
[20] J. Ziegler, *The Stopping and Ranges of Ions in Matter* (Pergamon Press, New York, 1977), Vol. 4.
[21] H. Gauvin, R. Bimbot, J. Herault, R. Anne, G. Bastin, and F. Hubert, Nucl. Instrum. Methods Phys. Res. B **28**, 191 (1987).
[22] H. A. Bethe and E. E. Salpeter, *Quantum Mechanics of One- and Two-Electron Atoms* (Plenum, New York, 1977).
[23] P. M. Echenique, R. H. Ritchie, and W. Brandt, Phys. Rev. B **20**, 2567 (1979).
[24] I. Despiney, D. Vernhet, J. P. Rozet, A. Chetioui, M. F. Politis, A. Touati, C. Stephan, L. Tassant-Got, A. Cassini, and J. P. Grandin, Radiat. Eff. Defects Solids **126**, 295 (1993).
[25] J. P. Rozet, A. Chetioui, P. Piquemal, D. Vernhet, K. Wohrer, C. Stephan, and L. Tassan-Got, J. Phys. B **22**, 33 (1989).